Trajectory Tracking Control for Electro-Optical Tracking System Using ESO Based Fractional-Order Sliding Mode Control

XINLI ZHOU AND XINGFEI LI

State Key Laboratory of Precision Measuring Technology and Instruments, Tianjin University, Tianjin 300072, China

Corresponding author: Xingfei Li (lixf_tju@163.com)

ABSTRACT In this study, to achieve high trajectory tracking performance in electro-optical tracking systems under strong nonlinear disturbances and uncertainties, we develop a nonlinear extended state observer (ESO) based fractional-order sliding mode control. When compared with previous work, the new compound control strategy is attractive in terms of the following three points. First, a novel controller is developed that integrates the advantages of a nonlinear ESO, a fractional-order nonsingular terminal sliding mode (FONTSM) manifold, and a super-twisting algorithm. Second, the nonlinear ESO is employed to estimate the disturbances and uncertainties without explicit knowledge of the system model. Third, a FONTSM manifold-based super-twisting algorithm is integrated into the controller to enhance the system robustness. The FONTSM manifold has a faster dynamical response, more flexible sliding manifold structure, and better control results than its integer-order NTSM counterpart. The finite-time convergences of the ESO and controller are both proved by the Lyapunov method. Finally, the comparative experimental results demonstrate the effectiveness and superiority of the developed control strategy with respect to existing approaches.

INDEX TERMS Electro-optical tracking system, extended state observer, nonsingular terminal sliding manifold, fractional-order, super-twisting algorithm.

I. INTRODUCTION

An electro-optical tracking system (EOTS) is a complex, high-accuracy device that is integrated with optical, mechanical, and electronic devices, and it has attracted increasing attention in recent decades [1], [2]. It has been widely used to expand the capabilities of humans in observation, surveillance, search and rescue, navigation, mapping, and optoelectronic countermeasure applications, to name a few, from civil to military domains [3]. To exploit the full potential of EOTSs, better control performance, clearer observation results, and longer monitoring distances are urgently required [4]. To achieve these goals, many trajectory tracking control methods [5]–[8], have been developed. The Line-of-sight stabilization control methods [9]–[11] have also been proposed.

The associate editor coordinating the review of this manuscript and approving it for publication was Zheng Chen.

However, although the abovementioned techniques are capable of achieving a certain performance, each of them has its limitations. Satisfactory tracking control is still hard to obtain for EOTS due to the strong nonlinear factors such as friction, uncertainties, disturbances, and model variation [3]. Thus, designing a novel control strategy for EOTS to tackle nonlinear factors is a challenging task that motivates us to do further research.

To tackle strong nonlinearities, many control methods were proposed such as SMC, adaptive backstepping method [12], model predictive control, fractional-order (FO) control and so on. SMC is a powerful technique for handling bounded disturbances and parameter uncertainties owing to its strong robustness and suitability for practical applications [13]–[15]. Nevertheless, chattering is a problem in SMC that cannot be neglected. Several methods have been proposed to reduce chattering, such as the nonsingular terminal sliding mode (NTSM) [16], high-order sliding mode

(HOSM) [17], observer compensation method [18], and reaching law method [19]. The NTSM method not only guarantees that the system state reaches its origin within a finite time, it also avoids the nonsingularity problem. In [20], to tackle unknown parameters, disturbances, and uncertainties, a robust adaptive NTSM method was developed for an automatic train operation system, and NTSM control with neural networks has been designed for MEMS gyroscopes [21]. HOSM methods such as the twisting algorithm, suboptimal algorithm, and super-twisting algorithm (STA) can reduce chattering and ensure finite-time convergence [22]. In particular, the STA, which handles a system state with a relative degree of one, is the most effective. It only requires the sliding manifold information, whereas other STAs require the sliding manifold derivative information as well. Because of the discontinuous function under the integral term, the chattering of the STA is greatly attenuated. In [23], a finite-time super-twisting SMC was proposed for Mars entry vehicles. A super-twisting SMC with adaptive gains and time delay estimation was proposed for maritime autonomous surface ships [24]. Moreover, an adaptive super-twisting sliding mode controller was designed for a wing-sweep morphing aircraft [25].

FO control is an effective control method that has become a new branch of automatic control. It can improve the flexibility of parameter adjustment and controller design. It has been broadly shown to be more effective than integer-order (IO) control and is always combined with various techniques such as SMC and PID control. In [26], a FO sliding mode controller with an FO disturbance observer was designed for UAVs and maglev suspension systems. In [27], to handle nonlinearities, a continuous FO nonsingular terminal sliding mode controller with dynamic SM manifold was designed for a class of second-order systems. A FO-based NTSM surface and a fast terminal sliding mode-type reaching law with time-delay estimation was proposed for a cable-driven manipulator [28]. To handle complex lumped uncertainties, a continuous FONTSM controller with time delay estimation was designed for cable-driven manipulators [29].

Moreover, since the time-varying lumped uncertainties existing in SMC are difficult to obtain, the observer technique is an effective approach to estimating them for a system and suppressing the chattering in SMC. Many proposed observers include the extended state observer (ESO) [30], disturbance observer [31], and finite-time disturbance compensator [32], [33] have achieved good effect. The ESO extends the system to a new state to estimate the lumped uncertainties and needs only the knowledge of inaccurate mathematical models for a strongly nonlinear system. It has been utilized in various applications, such as permanent magnet synchronous motor (PMSM) servo systems [34], hydraulic systems [35], rigid spacecraft systems [36], and mobile robots [37].

To the best of our knowledge, due to the complex uncertainties and disturbances in EOTS, it is difficult to implement high-performance tracking control using any of the existing control methods such as SMC, ESO-based methods, model-based methods, and PID. Therefore, a nonlinear ESO-based FO nonsingular terminal super-twisting SMC strategy is developed in this study. The motivation for developing compound control strategy is to reduce the impact of complex uncertainties and disturbances, thus achieving a satisfactory tracking control for EOTS. The novel compound controller is developed that integrates the advantages of a nonlinear ESO, a fractional-order nonsingular terminal sliding mode (FONTSM) manifold, and a super-twisting algorithm. The ESO is used to estimate lumped disturbances in real time without the need for accurate system models and disturbance models. The sliding mode dynamic, which utilizes a FONTSM manifold, has a more flexible control structure than the IO controller, and responds rapidly in both the sliding mode and reaching phases. The super-twisting technique is integrated into the FO sliding mode controller to reduce chattering and enhance robustness. The finite-time convergence of the designed ESO is demonstrated. The finite-time stability of the controller was also analyzed by the Lyapunov theorem. In addition to the developed novel ESO based SMC strategy, we performed experiments on the EOTS platform to evaluate its effectiveness. The contributions of this study are as follows:

1 An improved nonlinear function $\varphi(e_1(t))$ is employed in the ESO. The nonlinear ESO can estimate the lumped disturbance without requiring explicit information about the nonlinear factors and an accurate system model.

2 FO calculus is integrated with the NTSM manifold. The FONTSM manifold guarantees a fast dynamical response, avoids the nonsingularity problem, increases the sliding manifold flexibility, and achieves better control than the ordinary IO-based NTSM method.

3 A FONTSM manifold based super-twisting technique is integrated into the controller to improve the system robustness.

4 The finite-time stability of both the observer and the controller are analyzed via the Lyapunov theorem. Comparative experiments were carried out on the EOTS platform to demonstrate that the developed control strategy is effective and outperforms the existing NTSM [38], observer-based ISM [39], and ESO based super-twisting SMC [40] methods.

The remainder parts of this paper are organized as follows. In Section 2, the system model are introduced. Section 3 is devoted to describe the control design. Stability analysis of the developed control is given in Section 4. Experimental studies are given in Section 5. The conclusions are presented in Section 6.

Notations: For simplicity, we denote $\lfloor x \rceil^\alpha = sign(x)|x|^\alpha$ with $\alpha > 0$. $|\cdot|$ represents absolute value and $||\cdot||$ represents Euclidean norm.

II. PROBLEM STATEMENT AND SYSTEM MODEL

The system model of the EOTS is described as follows:

$$\begin{cases} \dot{\theta}_t = \omega_t \\ J\dot{\omega}_t = T_i + T_f + T_d \end{cases} \quad (1)$$

where θ_t and ω_t denote angle and angular velocity. J represents the moment of inertia. T_f indicates friction force. T_d indicates disturbances including external disturbance, uncertainties, and model variation. T_i is the electromagnetic force.

The system model (1) can be divided into two parts, the nominal part and the bias part, i.e., $J = J^* + \triangle J$, $T_f = T_f^* + \triangle T_f$, and $T_\triangle = T_\triangle^* + \triangle T_d$, where * is the nominal value and $\triangle$ is the difference between the real model and the nominal model. It worth noting that an EOTS always operates in a harsh environment. Wind disturbance and changes in aircraft attitude could lead to external disturbances and uncertainties $T_d^* + \triangle T_d$. Temperature variation and changes in the center of gravity could contribute to variation in the system model $\triangle J$ and $\triangle T_f$. Under such conditions, the trajectory tracking control performance will deteriorate significantly and the system may even become unstable.

Then the equation (1) can be reformulated as follows

$$J^* \dot{\omega}_t = T_i + h \quad (2)$$

where h denotes the lumped disturbance in EOTS,

$$h = T_f^* + \triangle T_f + T_d^* + \triangle T_d - \triangle J\dot{\omega}_t \quad (3)$$

It worth mention that EOTS is driven by permanent magnet synchronous motor (PMSM) directly. By using the field-oriented control (FOC) approach for PMSM, the electromagnetic force T_i could be described as follows:

$$T_i = \frac{3}{2}p\psi_d i_d = K_t i_d \quad (4)$$

where p denotes the number of pole pairs, ψ_d represents the permanent magnet flux linkages, K_t represents the torque coefficient and i_d is the driving current input.

Friction is one of the most complex nonlinear factors existing in EOTS. In this study, we adopt a modified friction model [41] with continuously differentiable characteristic to describe the friction behavior in EOTS. Owing to the using of a hyperbolic tangent and a differentiated Gaussian function, the modified friction model T_f is continuously differentiable with practical engineering value.

$$T_f = (T_s - T_c tanh(w_s/w_t) - \mu_s w_s)\frac{\dot{\theta}(t)}{w_s}e^{-(\frac{\dot{\theta}(t)}{\sqrt{2}})^2 + \frac{1}{2}} \\ + T_c tanh(\frac{\dot{\theta}(t)}{w_t}) + \mu_s \dot{\theta}(t) \quad (5)$$

where F_s denotes the Stribeck peak force, F_c represents the Coulomb friction force, μ_s indicates the viscous coefficient, w_s and w_t are the Stribeck and the transition velocity, respectively.

Let $x_1 = \theta_t$, $x_2 = \dot{\theta}_t$. The system model of EOTS in scalar form can be re-expressed as follows:

$$\begin{cases} \dot{x}_1(t) = x_2(t) \\ \dot{x}_2(t) = x_3(t) + b_0 u \end{cases} \quad (6)$$

where $b_0 = K_t/J^*$, $u = i_d$ and $x_3(t) = h/J^*$.

Thus, the objective we try to implement in this study can be described as: We design an effective controller u for the EOTS, to guarantee trajectory $x_1(t)$ to accurately and quickly track the predetermined reference trajectory $r(t)$ in the presence of complex uncertainties and disturbances, i.e., the tracking error $lim_{t\to\infty}\varepsilon_1(t) = lim_{t\to\infty}(x_1(t) - r(t)) = 0$.

Assumption 1: $\triangle T_f$, $\triangle T_d$, and $\triangle J$ are bounded. We assume that the lumped disturbance h and its derivative $\dot{h}$ exist and are bounded, satisfying $|h| \le \hbar \in \mathbb{R}^+$, where $\hbar$ is the unknown upper bound.

III. CONTROL DESIGN

In this section, the control design including ESO, FONTSM dynamic and super-twisting technique is described. A lemma is introduced to make the discussion more clearly.

Lemma 1 [42]: For dynamic system $\dot{x}_c = f(x_c(t))$ with $f(0) = 0$ and $x_c(t) \in \mathbb{R}^n$, assume that the following relationship between a positive define function $V_c(x_c(t))$ and its differential term are satisfied

$$\dot{V}_c(x_c(t)) \le -\tau_1 V_c(x_c(t)) - \tau_2 V_c(x_c(t))^\theta \quad (7)$$

where $\tau_1 > 0$, $\tau_2 > 0$ and $0 < \theta < 1$. The dynamic system is stable. Besides, the convergence time T_1 is obtained:

$$T_1 \le \frac{1}{\tau_1(1-\theta)} In \frac{\tau_1 V_c^{1-\theta}(x_c(t_0)) + \tau_2}{\tau_2} \quad (8)$$

where $V_c(x_c(t_0))$ is the initial value of $V_c(x_c(t))$. If $\tau_2 > 0$, $\tau_1 = 0$ with $0 < \theta < 1$, the dynamic system is still finite-time stable, the convergence time $T_2 \le \frac{1}{\theta\tau_2}V_c^\theta(x_c(t_0))$.

A. NONLINEAR ESO

A general linear ESO [40] for a second-order system can be presented as follows:

$$\begin{cases} \dot{z}_1(t) = z_2(t) - \beta_1 e_1(t) \\ \dot{z}_2(t) = z_3(t) - \beta_2 e_1(t) + b_0 u(t) \\ \dot{z}_3(t) = -\beta_3 e_1(t) \end{cases} \quad (9)$$

where β_1, β_2 and β_3 are the adjustable observer gains. $z_i(t)$ (i = 1,2,3) is the estimated value of the system states $x_i(t)$ (i = 1,2,3), respectively.

Consider the second-order system (6), an improved nonlinear ESO is designed as follows

$$\begin{cases} \dot{z}_1(t) = z_2(t) - \beta_1 \varphi(e_1(t)) \\ \dot{z}_2(t) = z_3(t) - \beta_2 \varphi(e_1(t)) + b_0 u(t) \\ \dot{z}_3(t) = -\beta_3 \varphi(e_1(t)) \end{cases} \quad (10)$$

The nonlinear function $\varphi(e_1(t))$ is presented as below:

$$\varphi(e_1(t)) = k_1 e_1(t) + k_2 \lfloor e_1(t) \rceil^{(r+1)/2} \quad (11)$$

where $k_1 > 0$, $k_2 > 0$, $0 < r < 1$.

In contrast to general linear ESOs, the designed nonlinear ESO includes a nonlinear function $\varphi(e_1(t))$. It combines the advantages of traditional linear and nonlinear ESOs. A detailed analysis is given in Remark 1.

The derivative of the function $\varphi(e_1(t))$ is given as follows:

$$\dot{\varphi}(e_1(t)) = (k_1 + k_2 \frac{r+1}{2} \lfloor e_1(t) \rceil^{(r-1)/2}) \dot{e}_1 \quad (12)$$

Define an intermediate variable Π

$$\Pi = k_1 + k_2 \frac{r+1}{2} \lfloor e_1(t) \rceil^{(r-1)/2} \quad (13)$$

So the Eq.(13) can be rewritten as

$$\dot{\varphi}(e_1(t)) = \Pi \dot{e}_1 \quad (14)$$

The observer error is defined as

$$\begin{cases} e_1(t) = z_1(t) - x_1(t) \\ e_2(t) = z_2(t) - x_2(t) \\ e_3(t) = z_3(t) - x_3(t) \end{cases} \quad (15)$$

Consider (6), (10) and (15), the observation error system is gained as follows

$$\begin{cases} \dot{e}_1(t) = e_2(t) - \beta_1 \varphi(e_1(t)) \\ \dot{e}_2(t) = e_3(t) - \beta_2 \varphi(e_1(t)) \\ \dot{e}_3(t) = \dot{h}(t) - \beta_3 \varphi(e_1(t)) \end{cases} \quad (16)$$

The proof of convergence of the nonlinear ESO is given in section IV.

B. INTRODUCTION TO FRACTIONAL ORDER CALCULUS AND FRACTIONAL ORDER CONTROL

The theoretical research into FO calculus dates back to about 300 years ago. However, its application has only gradually attracted increasing attention in recent years. The FO differentiation and integration operators, which can be thought of as generalizations of their IO versions, are defined as follows:

$$_{t_0}\mathcal{R}_t^\alpha = \begin{cases} \dfrac{d^\alpha}{dt^\alpha}, & \Re(\alpha) > 0 \\ 1, & \Re(\alpha) = 0 \\ \int_{t_0}^t (d\tau)^{-\alpha}, & \Re(\alpha) < 0 \end{cases} \quad (17)$$

where $\mathcal{R}$ represents the fractional calculus; α represents the fractional order value; t_0 and t indicate the limits for the operator; and $\Re(\alpha)$ means the real part of α.

As the development of FO calculus theory, the FO definition is diverse. The three most commonly used fractional order calculus definitions in engineering application field are Riemann-Liouville (RL), Grunwald-Letnikov (GL) and Caputo. It worth noting that the proposed controller in this paper is developed according to Caputo definition. The definition for Caputo FO calculus is expressed as follows

$$_{t_0}\mathcal{R}_t^\alpha f(t) = \frac{1}{\Gamma(m-\alpha)} \int_{t_0}^t \frac{f^m(\tau)}{(t-\tau)^{\alpha+1-m}} d\tau$$
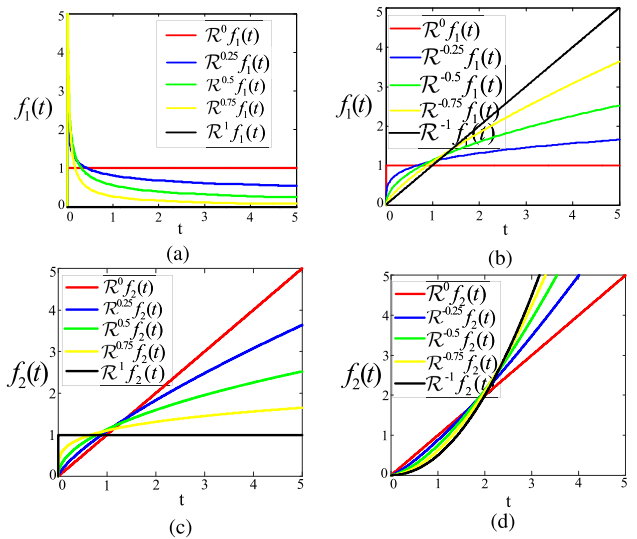$$(m-1 \le \alpha < m) \quad (18)$$

FIGURE 1. FO function $f_1(t) = 1$ and $f_2(t) = t$. (a) $f_1(t)$ FO differential. (b) $f_1(t)$ FO integral. (c) $f_2(t)$ FO differential. (d) $f_2(t)$ FO integral.

in which m represents an integer, and $\Gamma(\cdot)$ means the Gamma function $\Gamma(\gamma) = \int_0^\infty e^{-t} t^{\gamma-1} dt$.

In term of the amplitude-frequency characteristic, the Laplace transform is adopted to describe the FO calculus. The Laplace transform for Caputo FO calculus is expressed as below:

$$\mathscr{L}\{_{t_0}\mathcal{R}_t^{\pm\alpha} f(t)\} = \int_0^\infty e^{-st} {}_{t_0}\mathcal{R}_t^{\pm\alpha} f(t) = s^{\pm\alpha} \mathcal{L}\{f(t)\} \quad (19)$$

where $s = j\omega$ means the Laplace transform variable. Besides, it is worth mentioning that a fractional-order controller is able to adjust the slope of the Bode diagram shape arbitrarily, whereas the IO controller can only adjust its slope by integer multiples of 20 dB/decade.

To illustrate the different results of IO and FO calculus, two typical functions $f_1(t) = 1$ and $f_2(t) = t$ are introduced as follows:

C. FRACTIONAL-ORDER NONSINGULAR TERMINAL SUPER-TWISTING CONTROLLER

The tracking error is defined as below:

$$\begin{cases} \varepsilon_1(t) = x_1(t) - r(t) \\ \varepsilon_2(t) = x_2(t) - \dot{r}(t) \end{cases} \quad (20)$$

where $\varepsilon_1(t)$ and $\varepsilon_2(t)$ are angle tracking error and angle rate tracking error, respectively. $r(t)$ is the reference trajectory and it is twice differentiable, continuous and bounded.

By employing the derivative on (20), the tracking error system is obtained as

$$\begin{cases} \dot{\varepsilon}_1(t) = \varepsilon_2(t) \\ \dot{\varepsilon}_2(t) = h(t) + b_0 u(t) - \ddot{r}(t) \end{cases} \quad (21)$$

Consider the following fractional-order nonsingular terminal sliding manifold $s \in \mathbb{R}^n$:

$$s = \dot{\varepsilon}_1 + \alpha_1 \mathcal{R}^{\chi_1} \lfloor \varepsilon_1 \rceil^{\gamma_1} + \alpha_2 \mathcal{R}^{\chi_2-1} \lfloor \varepsilon_1 \rceil^{\gamma_2} \quad (22)$$

where parameters $\alpha_1, \alpha_2, \chi_1, \chi_2, \gamma_1, \gamma_2$ are positive.

Differentiating on both sides of the sliding manifold (22), the following equation is gotten:

$$\begin{aligned} \dot{s} &= \dot{\varepsilon}_2 + \alpha_1 \mathcal{R}^{\chi_1+1} \lfloor \varepsilon_1 \rceil^{\gamma_1} + \alpha_2 \mathcal{R}^{\chi_2} \lfloor \varepsilon_1 \rceil^{\gamma_2} \\ &= h(t) + b_0 u(t) - \ddot{r}(t) \\ &\quad + \alpha_1 \mathcal{R}^{\chi_1+1} \lfloor \varepsilon_1 \rceil^{\gamma_1} + \alpha_2 \mathcal{R}^{\chi_2} \lfloor \varepsilon_1 \rceil^{\gamma_2} \end{aligned} \quad (23)$$

When neglecting the lumped disturbance $h(t)$, by setting $\dot{s} = 0$, the equivalent controller is obtained as follows

$$u_{eq} = \frac{1}{b_0}(\ddot{r}(t) - \alpha_1 \mathcal{R}^{\chi_1+1} \lfloor \varepsilon_1 \rceil^{\gamma_1} - \alpha_2 \mathcal{R}^{\chi_2} \lfloor \varepsilon_1 \rceil^{\gamma_2}) \quad (24)$$

A generalized super-twisting algorithm [44] which could provide more robustness and faster convergence rate than standard super-twisting algorithm is adopted.

$$u_{st} = \frac{1}{b_0}(-K_1 \phi_1(s) - K_2 \int_0^t \phi_2(s) dt) \quad (25)$$

where $\phi_1(s)$ and $\phi_2(s)$ denote nonlinear functions with extra linear correction terms based on [44]

$$\begin{cases} \phi_1(s) = \lfloor s \rceil^{1/2} + s \\ \phi_2(s) = \frac{1}{2} sign(s) + \frac{3}{2} \lfloor s \rceil^{1/2} + s, \end{cases} \quad (26)$$

$K_1 > 0, K_2 > 0$.

Consider the equivalent controller, the generalized super-twisting algorithm and the ESO, the control input u is designed containing three components u_{eq}, u_{st} and u_{ob}

$$u = u_{eq} + u_{st} + u_{ob}$$

$$\begin{cases} u_{eq} = \frac{1}{b_0}(\ddot{r}(t) - \alpha_1 \mathcal{R}^{\chi_1+1} \lfloor \varepsilon_1 \rceil^{\gamma_1} - \alpha_2 \mathcal{R}^{\chi_2} \lfloor \varepsilon_1 \rceil^{\gamma_2}) \\ u_{st} = \frac{1}{b_0}(-K_1 \phi_1(s) - K_2 \int_0^t \phi_2(s) dt) \\ u_{ob} = -\frac{z_3}{b_0} \end{cases} \quad (27)$$

By substituting (27), (28) into (23), the sliding manifold dynamic system can be expressed as

$$\dot{s} = -K_1 \phi_1(s) - K_2 \int_0^t \phi_2(s) dt - e_3 \quad (28)$$

where $e_3 = z_3 - h(t)$. Define z_{s1} and z_{s2} as the new state

$$\begin{cases} z_{s1} = s \\ z_{s2} = -K_2 \int_0^t \phi_2(s) dt - e_3 \\ \dot{e}_3 = -\dot{h}(t) - \beta_3 \varphi(e_1) = -\rho \end{cases} \quad (29)$$

Then the closed-loop system dynamic in scalar form can be written as

$$\begin{cases} \dot{z}_{s1} = -K_1 \phi_1(s) + z_{s2} \\ \dot{z}_{s2} = -K_2 \phi_2(s) + \rho \end{cases} \quad (30)$$

According to Theorem 1, the observer error system is finite-time bounded. So supposed $|\rho| \le \varrho$ with $\varrho \in \mathbb{R}^+$.
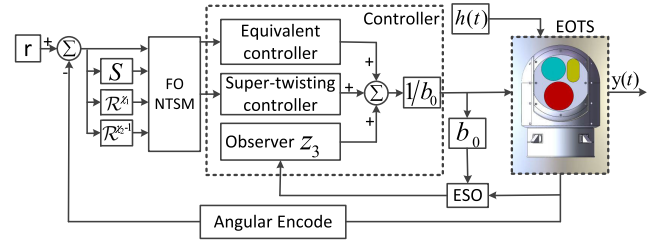

FIGURE 2. Control block diagram.

Afterwards, the developed control strategy (27)(28) is presented in Fig.2.

The proof of stability of the controller based on super-twisting algorithm is given in section IV.

IV. STABILITY ANALYSIS
A. CONVERGENCE OF ESO

Theorem 1: Consider the designed ESO (10) with Assumption 1, there exist suitable parameters β_i (i = 1,2,3) and k_1, k_2, r such that

$$\begin{cases} \beta_i > 0(i = 1, 2, 3), k_1 > 0, k_2 > 0, 0 < r < 1 \\ \Pi \beta_1 \beta_2 - \beta_3 > 0 \end{cases} \quad (31)$$

is satisfied. The observation error system (16) converges to zero in a finite time.

Proof: A Lyapunov candidate function is selected as

$$V_e = \eta^T P \eta \quad (32)$$

where $\eta = [\varphi(e_1(t)), e_2(t), e_3(t)]^T$ and the matrix P with nonsingular and symmetric features is expressed as

$$P = \begin{bmatrix} \beta_1^2 + \beta_2^2 + \beta_3^2 & -\beta_2 & -\beta_3 \\ -\beta_2 & 2 & 0 \\ -\beta_3 & 0 & 2 \end{bmatrix}. \quad (33)$$

Then V_e can be calculated as

$$\begin{aligned} V_e &= \beta_1^2 \varphi^2(e_1(t)) + e_2^2(t) + e_3^2(t) + (\beta_2 \varphi^2(e_1(t)) \\ &\quad - e_2(t))^2 + (\beta_3 \varphi^2(e_1(t)) - e_3(t))^2 \ge 0 \end{aligned} \quad (34)$$

where V_e is continuous and continuously differentiable everywhere when $e_1(t) \ne 0$.

Taking the derivative of η with respect to time:

$$\begin{aligned} \dot{\eta} &= \begin{bmatrix} \Pi(e_2(t) - \beta_1 \varphi(e_1(t))) \\ e_3(t) - \beta_2 \varphi(e_1(t)) \\ -\dot{h}(t) - \beta_3 \varphi(e_1(t)) \end{bmatrix} \\ &= A\eta + B\dot{h}(t) \end{aligned} \quad (35)$$

with

$$A = \begin{bmatrix} -\beta_1 & 1 & 0 \\ -\beta_2 & 0 & 1 \\ -\beta_3 & 0 & 0 \end{bmatrix}, B = \begin{bmatrix} 0 \\ 0 \\ 1 \end{bmatrix}.$$

The characteristic polynomial of A is obtained as

$$G(\zeta) = |\zeta I - A| = \zeta^3 + \beta_1 \Pi \zeta^2 + \beta_2 \Pi \zeta + \beta_3 \Pi \quad (36)$$

where ζ is a Laplase variable. The observer gains β_i ($i = 1,2,3$), intermediate variable Π, and parameters k_1, k_2 should satisfy the conditions (32) such that A is a Hurwitz matrix and all coefficients of $G(\zeta)$ are positive.

Employing the derivative of V_e yields:

$$\begin{aligned}
\dot{V}_e &= \dot{\eta}^T P \eta + \eta^T P \dot{\eta} \\
&= (A\eta + B\dot{h}(t))^T P \eta + \eta^T P (A\eta + B\dot{h}(t)) \\
&= \eta^T (A^T P + PA)\eta + 2\dot{h}^T(t) M_0 \eta
\end{aligned} \quad (37)$$

where $M_0 = -B^T P = [\beta_3, 0, -2]$. Let $M = ||M_0|| = \sqrt{\beta_3^2 + 4}$, and $|\dot{h}^T(t)| \leq H$. Since matrix A is pointwise Hurwitz, there exists positive definite matrix Q which satisfies the following equation.

$$A^T P + PA = -Q. \quad (38)$$

A inequality based on (33) can be presented as follows

$$\lambda_{min}\{P\}||\eta||^2 \leq V_e \leq \lambda_{max}\{P\}||\eta||^2 \quad (39)$$

with $||\eta||^2 = \varphi^2(e_1(t)) + e_2^2(t) + e_3^2(t)$.

Then, according to (39), the derivative of V_e is rewritten as

$$\begin{aligned}
\dot{V}_e &\leq -\eta^T Q \eta + 2\dot{h}^T M_0 ||\eta|| \\
&\leq -\lambda_{min}\{Q\}||\eta||^2 + 2HM||\eta|| \\
&= -\frac{1}{2}(\lambda_{min}\{Q\}||\eta|| - 4HM)||\eta|| - \frac{1}{2}\lambda_{min}\{Q\}||\eta||^2.
\end{aligned} \quad (40)$$

Note that the inequality $||\eta|| \geq \frac{4HM}{\lambda_{min}\{Q\}}$ is guaranteed by properly selecting the parameters, the $\dot{V}_e \leq 0$. Particularly, according to (41), when $||\eta|| \geq \frac{4HM}{\nu\lambda_{min}\{Q\}}$ with $0 < \nu < 1$ is guaranteed, one has that

$$\dot{V}_e \leq -\lambda_1 ||\eta||^2 - \lambda_2 ||\eta|| \quad (41)$$

where $\lambda_1 = -\frac{1}{2}\lambda_{min}\{Q\}$, $\lambda_2 = \frac{2HM(1-\nu)}{\nu}$.

Substituting (40) into (42), and yields

$$\dot{V}_e \leq \frac{\lambda_1}{\lambda_{max}\{P\}} V_e - \frac{\lambda_2}{\sqrt{\lambda_{max}\{P\}}} \sqrt{V_e}. \quad (42)$$

According to Lemma 1, the observation error (15) is able to converge into the region $\{||\eta|| \geq \frac{4HM}{\lambda_{min}\{Q\}}\}$ within finite time T_1. Besides, the upper reaching time is presented as follows

$$T_1 \leq \frac{2\lambda_{max}\{P\}}{\lambda_1} In \frac{\frac{\lambda_1}{\lambda_{max}\{P\}}\sqrt{V_e(0)} + \frac{\lambda_2}{\sqrt{\lambda_{max}\{P\}}}}{\frac{\lambda_2}{\sqrt{\lambda_{max}\{P\}}}} \quad (43)$$

where $V_e(0)$ is the initial value of $V_e(e(t))$. This completes the proof.

B. CONVERGENCE OF THE CLOSED-LOOP SYSTEM

Theorem 2: Assume that there exist a positive and symmetric definite matrix $\Upsilon = \Upsilon^T > 0$ such that the matrix inequality (45) or Algebraic Riccati Inequality (46)

$$\begin{bmatrix} \Lambda^T \Upsilon + \Upsilon \Lambda + \epsilon \Upsilon + R & \Upsilon B_s + S^T \\ B_s^T \Upsilon + S & -\bigstar \end{bmatrix} \leq 0 \quad (44)$$

$$\begin{aligned}
&\Lambda^T \Upsilon + \Upsilon \Lambda + \epsilon \Upsilon + R \\
&+ (\Upsilon B_s + S^T)\bigstar^{-1}(B_s^T \Upsilon + S) \leq 0
\end{aligned} \quad (45)$$

is satisfied. Then trajectories of the system state (30) converge to origin in a finite time less than T_2 for all bounded perturbations satisfying $|\rho| \leq \varrho$.

$$T_2 = \frac{2}{\epsilon} In(\frac{2}{\sqrt{\lambda_{max}\{\Upsilon\}}} V_s^{1/2}(t_0) + 1). \quad (46)$$

Proof: A Lyapunov function is considered as follows

$$V_s = \xi^T \Upsilon \xi \quad (47)$$

where $\xi = [\phi_1(z_{s1}), z_{s2}]^T$. And $\Upsilon = \Upsilon^T > 0$ is a positive definite, symmetric matrix and radially unbounded function in $\mathbb{R}^2$. Note that $\phi_2(z_{s1}) = \phi_1(z_{s1})\phi_1'(z_{s1})$, and $\phi_1'(z_{s1}) = (\lfloor z_{s1} \rceil^{1/2} + z_{s1})$. Then $\dot{\xi}$ can be expressed as

$$\begin{aligned}
\dot{\xi} &= \phi_1'(z_{s1}) \begin{bmatrix} -K_1\phi_1(z_{s1}) + z_{s2} \\ -K_2\phi_1(z_{s1}) + \frac{\rho}{\phi_1'(z_{s1})} \end{bmatrix} \\
&= \phi_1'(z_{s1})(\Lambda\xi + B_s\widetilde{\rho})
\end{aligned} \quad (48)$$

where

$$\Lambda = \begin{bmatrix} -K_1 & 1 \\ -K_2 & 0 \end{bmatrix}, B_s = \begin{bmatrix} 0 \\ 1 \end{bmatrix}.$$

According to [44], a transformed perturbation $\widetilde{\rho}(t, \xi)$, $t > 0$ is satisfied with a sector condition for all $\widetilde{\rho} \in \mathbb{R}^2$ as follows:

$$\omega(\xi, \widetilde{\rho}) = \begin{bmatrix} \xi \\ \widetilde{\rho} \end{bmatrix}^T \begin{bmatrix} R & S^T \\ S & -\bigstar \end{bmatrix} \begin{bmatrix} \xi \\ \widetilde{\rho} \end{bmatrix} \quad (49)$$

where R, $\bigstar$ are two positive constants, and $S = [m \quad n]$, m, n are two constants.

A standard inequality is given as follows according to (48)

$$\lambda_{min}\{\Upsilon\}||\xi||^2 \leq V_s \leq \lambda_{max}\{\Upsilon\}||\xi||^2 \quad (50)$$

where $||\xi||^2 = \phi_1^2(z_{s1}) + z_{s2}^2 = |z_{s1}| + 2|z_{s1}|^{3/2} + |z_{s1}|^2 + z_{s2}^2$. Then the following equation is gained

$$|z_{s1}|^{1/2} \leq ||\xi|| \leq \frac{V_s^{1/2}(s)}{\lambda_{min}^{1/2}\{\Upsilon\}} \quad (51)$$

The derivative of the Lyapunov function is

$$\begin{aligned}
\dot{V}_s &= \dot{\xi}^T \Upsilon \xi + \xi^T \Upsilon \dot{\xi} \\
&= \{\xi^T(\Lambda^T \Upsilon + \Upsilon \Lambda)\xi + \widetilde{\rho}^T B_s^T \Upsilon \xi + \xi^T \Upsilon B_s \widetilde{\rho}\} \\
&= \phi_1'(z_{s1}) \begin{bmatrix} \xi \\ \widetilde{\rho} \end{bmatrix}^T \begin{bmatrix} \Lambda^T \Upsilon + \Upsilon \Lambda & \Upsilon B_s \\ B_s^T \Upsilon & 0 \end{bmatrix} \begin{bmatrix} \xi \\ \widetilde{\rho} \end{bmatrix} \\
&\leq \phi_1'(z_{s1})(\begin{bmatrix} \xi \\ \widetilde{\rho} \end{bmatrix}^T \begin{bmatrix} \Lambda^T \Upsilon + \Upsilon \Lambda & \Upsilon B_s \\ B_s^T \Upsilon & 0 \end{bmatrix} \begin{bmatrix} \xi \\ \widetilde{\rho} \end{bmatrix} + \omega(\xi, \widetilde{\rho})) \\
&= \phi_1'(z_{s1}) \begin{bmatrix} \xi \\ \widetilde{\rho} \end{bmatrix}^T \begin{bmatrix} \Lambda^T \Upsilon + \Upsilon \Lambda + R & \Upsilon B_s + S^T \\ B_s^T \Upsilon + S & -\bigstar \end{bmatrix} \begin{bmatrix} \xi \\ \widetilde{\rho} \end{bmatrix} \\
&\leq -\phi_1'(z_{s1})\epsilon V_s = -\frac{1}{2|z_{s1}|^{1/2}}\epsilon V_s - \epsilon V_s \\
&\leq -\frac{\epsilon\lambda_{min}^{1/2}\{\Upsilon\}}{2} V_s^{1/2} - \epsilon V_s
\end{aligned} \quad (52)$$

where $\epsilon > 0$, $\lambda_{min}^{1/2}\{\Upsilon\} > 0$. Thus, $\dot{V}_s \leq 0$ holds. Since the inequality above resembles with the inequality (7), according

to lemma 1, the controller is capable of steering the system state to zero in a time less than T_2 (47).

Remark 1: Nonlinear function $\varphi(e_1(t))$ (11) consists of two parts $k_1 e_1(t)$ and $k_2 \lfloor e_1(t) \rceil^{(r+1)/2}$. When $k_1 = 1$ and $k_2 = 0$, the designed nonlinear ESO reduces to the general linear ESO (9). Note that the second term $k_2 \lfloor e_1(t) \rceil^{(r+1)/2}$ in (11) is based on an continuous finite-time convergent differentiator technique and exhibits a better chattering suppression performance and a better observation accuracy than traditional sliding mode observation [43]. For instance, if $k_1 e_1(t) > k_2 \lfloor e_1(t) \rceil^{(r+1)/2}$ when the error system is far away from zero, the term $k_1 e_1(t)$ in (11) dominates. In contrast, if $k_1 e_1(t) < k_2 \lfloor e_1(t) \rceil^{(r+1)/2}$ when the error system is very close to zero, the second term in (11) dominates. Thus, the appropriate selection of parameters r, k_1, and k_2 according to the application will improve the results.

Remark 2: The FO differentiation and integration operators can be regarded as generalizations of their IO versions. The designed FO sliding manifold is better than the IO ones since that it is able to increase the degrees of freedom of the sliding mode controller and the parameter adjustment is more flexible, thus yielding better robustness and tracking accuracy. It can be seen that when $\chi_1 = 1$ and $\chi_2 = 0$, the FONTSM manifold $s = \dot{\varepsilon}_1 + \alpha_1 \mathcal{R}^{\chi_1} \lfloor \varepsilon_1 \rceil^{\gamma_1} + \alpha_2 \mathcal{R}^{\chi_2-1} \lfloor \varepsilon_1 \rceil^{\gamma_2}$ is degenerates to its special IO form $s = \dot{\varepsilon}_1 + \alpha_1 d \lfloor \varepsilon_1 \rceil^{\gamma_1} / dt + \alpha_2 \int \lfloor \varepsilon_1 \rceil^{\gamma_2} dt$. Because that the additional parameters χ_1 and χ_2 can be set arbitrarily, the designed FO controller outperforms the IO controller in term of control accuracy and robustness.

Remark 3: In the upper region of observation error $\|\eta\| \geq \frac{4HM}{\lambda_{min}\{Q\}}$, because $M = \|M_0\| = \sqrt{\beta_3^2 + 4}$, and $|\dot{h}^T(t)| \leq H$, the value of numerator $4HM$ depends on the parameter β_3. Moreover, the denominator $\lambda_{min}\{Q\}$ relies on parameters β_1, β_2, β_3 and r. Thus, when the parameter β_3 is set correctly, the numerator can be treated as a constant. Subsequently, we can adjust β_1, β_2 and r to satisfy the condition (32) and make the value of the denominator as large as possible. Note that the upper region of the observation error $\|\eta\|$ can be decreased to a small and negligible value, hence, the observed accuracy of the nonlinear ESO is sufficient.

V. EXPERIMENTAL STUDIES
A. EXPERIMENTAL SETUP
The experimental setup is depicted in Fig.3. It contains mainly four parts: personal computer (PC), power supply (24V), digital signal processor (DSP) controller and EOTS. The schematic diagram of EOTS is presented in Fig.4, which includes infrared camera, visible light television camera, PMSM, driver magnetic Encoder (RENISHAW AksIM with 0.01° measurement accuracy).

The reference trajectory is given by a personal computer (PC). The DSP controller receives the reference signals, implements the proposed algorithm (Period: 1ms), and sends the algorithm result to the motor driver. Next, the motor driver amplifies the algorithm's output and drives the PMSM in
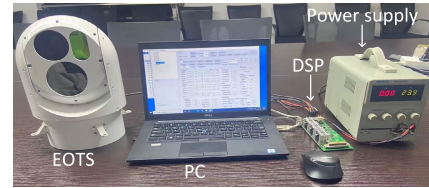

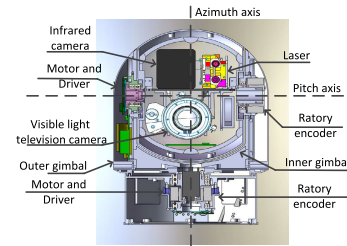**FIGURE 3.** The experimental setup.

FIGURE 4. The schematic diagram of EOTS.

the azimuth axis to track the desired trajectory. Additionally, the FO terms in controller is implemented by the oustaloup filter approximation method. The order of oustaloup filter is selected as five order and the frequency range is choose as 0.001-100 rad/s.

1) CONTROLLER PARAMETERS
The method of selecting the parameters consists of the following three steps. First, we determined the parameters of the ESO. The selection of β_{1-3}, k_{1-2}, and r for estimating the lumped disturbance can substantially affect the control performance. A large β_{1-3} indicates a large bandwidth, but if it is too large, this leads to serious chattering in the control results, whereas a value of β_{1-3} that is too small cannot ensure stability. Hence, we selected the set of β_{1-3} and r shown in Table 1 to ensure the accuracy of the observed value without much chattering. We also adjusted k_{1-2} to reduce the observed error slightly. Second, we determined the parameters of the fractional-order nonsingular terminal sliding manifold. The fractional-integral term $\mathcal{R}^{\chi_2-1}$ can be regarded as a low-pass filter. The value of χ_2 is selected so that the steady-state errors are reduced. However, a value of χ_2 that is too large will cause long-term integration, which could result in a steady-state oscillations. Suitable values of α_2 and γ_2, as listed in Table 1, will further reduce the steady-state errors. For the fractional-differential term $\mathcal{R}^{\chi_1}$, the values of the fractional-differential parameter χ_1 together with those of α_2 and γ_2 listed in Table 1 are able to ensure

TABLE 1. Controller parameters.

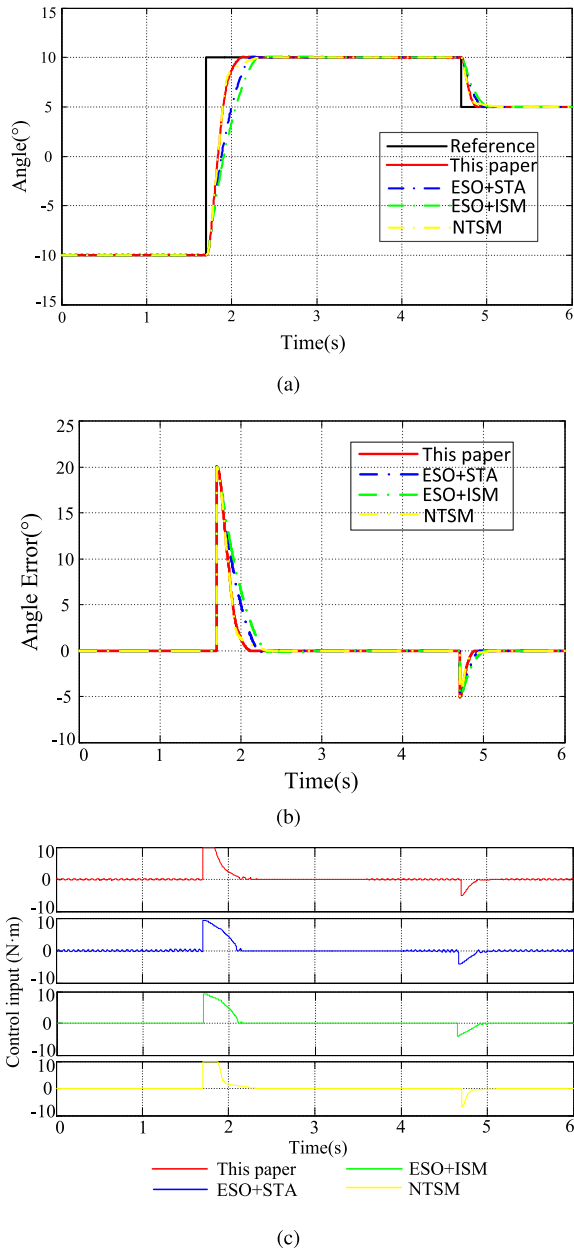| Parameter	Value	Parameter	Value	Parameter	Value
β_1	800	β_2	2400	β_3	3500
r	0.5	α_1	6	χ_1	0.01
γ_1	0.85	χ_2	0.99	γ_2	0.85
α_2	0.2	K_1	1.5	K_2	7
b_0	30	k_1	1	k_2	0.3

(a)

(b)

(c)

FIGURE 5. Results of the step trajectory experiment.

rapid response without overshoot. Third, the parameters of u_{st} were determined. An appropriate value of K_{1-2} can enhance the robustness. However, a value that is too large may lead to chattering. When the load changes, we can re-adjust the value of K_{1-2} to handle it. Finally, based on the above discussion, we selected a set of parameters to ensure high tracking accuracy, good robustness, and rapid response. The values are listed in Table 1.

2) EXPERIMENTS

The following four control methods are taken for experimental comparison: Our developed control strategy;

(a)

(b)

(c)

(d)

(e)
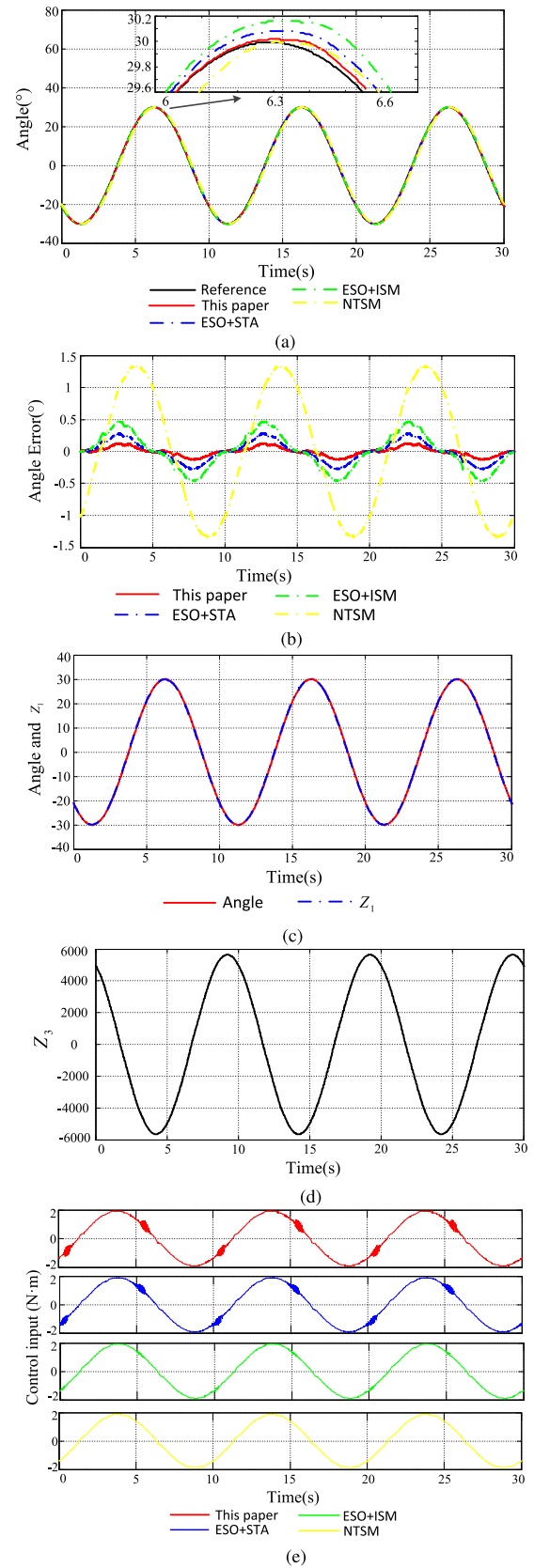
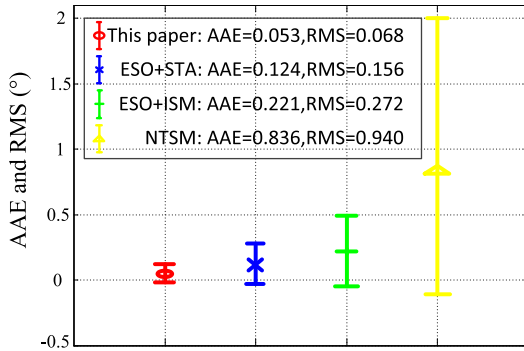**FIGURE 6.** Results of the sinusoidal trajectory experiment.

FIGURE 7. AAE and RMS of the sinusoidal trajectory experiment.

The NTSM control method [38]; The ESO based integral sliding mode (ESO+ISM) method [39]; The ESO based super-twisting sliding mode (ESO+STA) method [40].

The following four experiments were designed to evaluate the effectiveness of the developed method. In the first experiment, a step reference trajectory with two angles was designed to evaluate the response speed. In the second experiment, a sinusoidal reference trajectory was tested, and in the third experiment, a triangular reference trajectory with two angular velocities was employed. A higher angular velocity indicates increased friction, enabling the friction compensation to be evaluated. In the fourth experiment, a 2 kg load was added to the EOTS with the same triangular reference trajectory used in the third experiment to check the robustness of the system against uncertainties.

Furthermore, to make the compared results more convincing, the following calculations are introduced: the absolute average error $\text{AAE} = \frac{1}{N}\sum_{i=1}^{N}|\varepsilon_1(i)|$ and the root-mean-square error $\text{RMS} = \sqrt{\sum_{i=1}^{N}\frac{\varepsilon_1^2(i)}{N}}$.

B. EXPERIMENTAL RESULTS

1) STEP REFERENCE TRAJECTORY

In the first experiment, a step signal with two amplitudes, 5° and 20°, is used as the predetermined reference trajectory. The corresponding experimental results are shown in Figs.5(a)-(c). Fig.5(a) shows the tracking results, and Fig.5(b) presents the tracking errors. All four control methods are able to track the step reference trajectory accurately without any overshoot, while still converging quickly. In particular, because of the adopted FONTSM manifold, our proposed control strategy is faster than the other three control methods for both the 5° and 20° signals. Fig.5(c) presents the four control inputs. To avoid the actuator saturation, the maximal control input is limited to 10 $N \cdot m$ by the motor driver. Actuator saturation is considered in the case of 20° and ignored in the case of 5°. Analyzing the 20° results further, our proposed control strategy has a shorter response time (0.412 s) than the ESO+STA (0.562 s), ESO+ISM
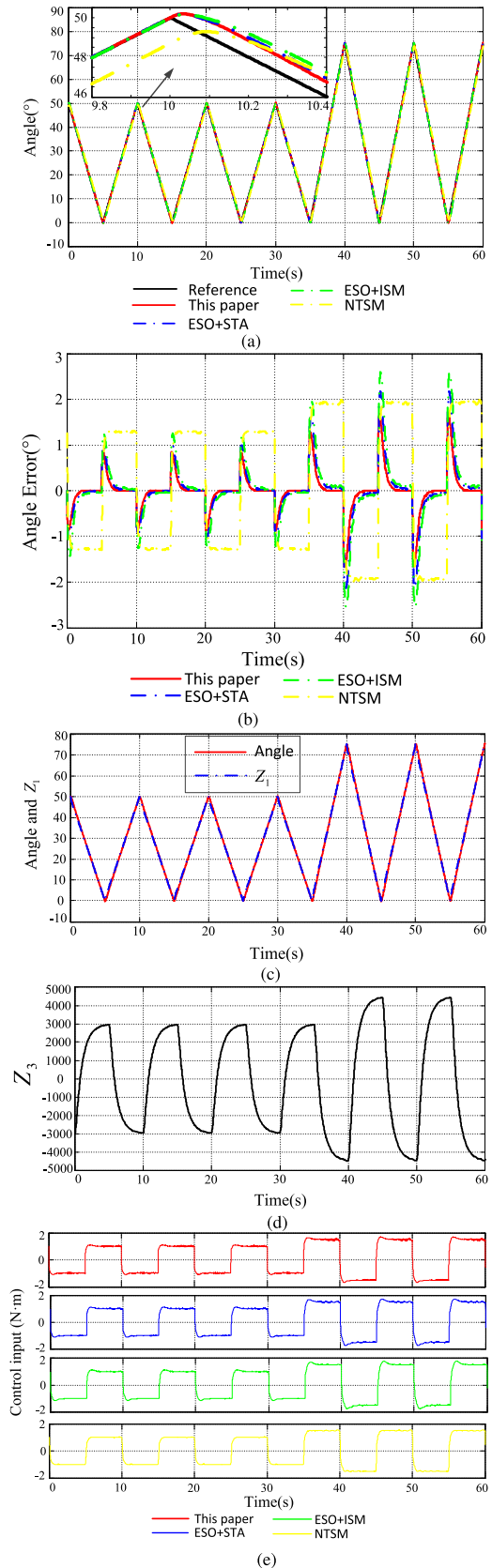

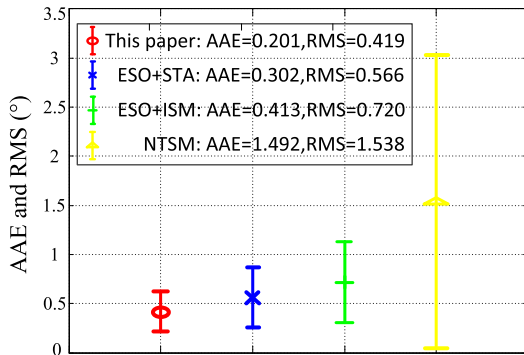**FIGURE 8.** Results of the triangular trajectory experiment.

FIGURE 9. AAE and RMS of the triangular trajectory experiment.

(0.544 s), and NTSM (0.566 s) methods. The results of the step trajectory experiment are compared in Table 2.

**TABLE 2.** Comparison results of the step trajectory experiment.

| Controller	This paper	ESO+STA	ESO+ISM	NTSM
Response time	0.412 s	0.512 s	0.584 s	0.577 s

2) SINUSOIDAL REFERENCE TRAJECTORY

In the second experiment, a sinusoidal angle with a peak amplitude of 30° and frequency of 0.1 Hz was used as the predetermined reference trajectory. The corresponding experimental results are shown in Figs. 6(a)-(e). In Fig.6(a), the four control approaches are all capable of tracking the predetermined sinusoidal reference trajectory with very little error. Fig.6(b) shows the tracking errors of the four approaches. The maximal error peak occurs when the system reaches the peak angle amplitude and changes direction. This is caused by changes in the system from static friction to dynamic friction. Because of the STA with the FONTSM manifold, the error peaks converge to zero more rapidly than in the other three methods. Owing to the designed ESO and the super-twisting controller with the FONTSM manifold, the proposed control strategy yields the smallest tracking error over the entire motion procedure. Specifically, for AAE, the one yielded by the developed control scheme is 42.8%, 24.0% and 6.3% of the ones by the ESO+STA, ESO+ISM, and NTSM methods, respectively. For RMS, the result is 43.6%, 25.1%, and 7.2% of results for the ESO+STA, ESO+ISM, and NTSM method, respectively. Fig.6(c) shows that the observed result of z_1 is easily able to capture the real angle. Fig.6(d) shows the lumped disturbance z_3, and Fig. 6(e) shows the control efforts. The AAE and RMS values of the comparative results of the four methods are shown in Fig.7.

3) TRIANGULAR REFERENCE TRAJECTORY

In the third experiment, a triangular signal with two angular velocities of $10°/s$ and $15°/s$ is used as the predetermined reference trajectory. The corresponding experimental results are shown in Figs.8(a)-(e). The results in Fig.8(a) show that the four control methods are able to track the predetermined triangular reference trajectory with small errors. Fig.8(b) presents the four tracking errors. The proposed nonlinear
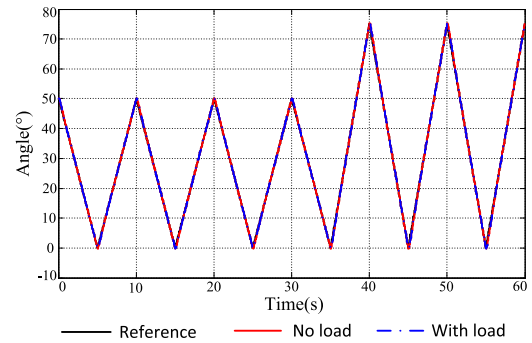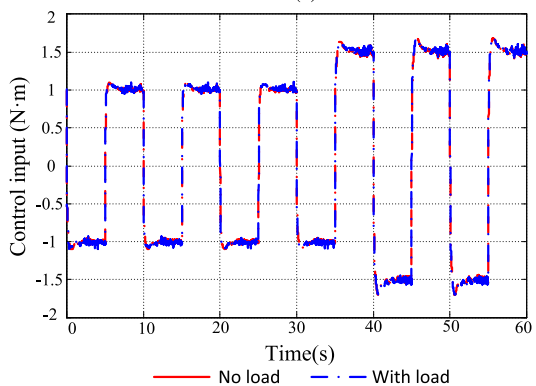

(a)
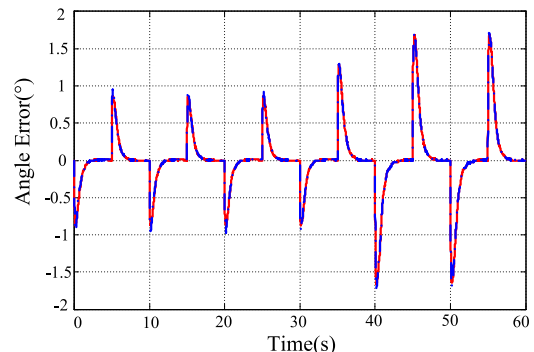
(b)
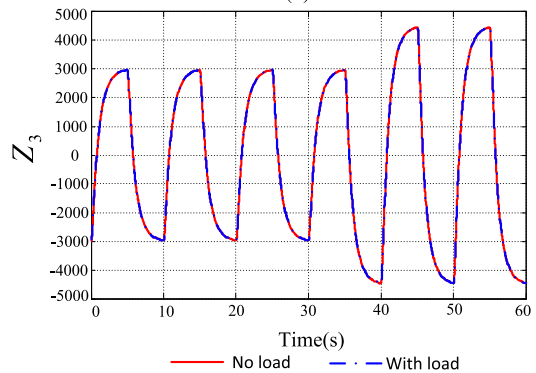
(c)

(d)

FIGURE 10. Results of the triangular trajectory with load experiment.

ESO enables the developed control strategy to achieve the smallest tracking error when the system is in the uniform motion period. The maximal error peak occurs when the
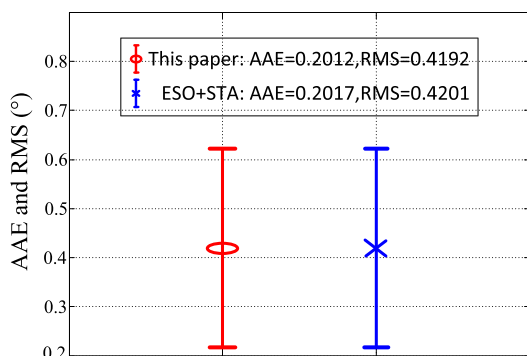
FIGURE 11. AAE and RMS of the triangular trajectory with load experiment.

system is changing direction. Again, this is caused by changes in the system from static friction to dynamic friction. Owing to the proposed STA with the FONTSM manifold, the error peaks converge to zero more quickly than for the other three methods. Obviously, as the angular velocity increases, the four tracking performances all degrade, which is caused by the increased friction. However, the increase in tracking error of the proposed control strategy is the smallest, and this strategy performs the best over the entire tracking process, regardless of whether the system is moving uniformly or changing direction. Specifically, for AAE, the one yielded by the developed control strategy is 53.6%, 32.1%, and 4.88% of the ones by the ESO+STA, ESO+ISM, and NTSM methods, respectively. For RMS, the result is 66.2%, 44.5%, and 13.7% of the results of the ESO+STA, ESO+ISM, and NTSM methods. Fig.8(c) shows that the observed result of z_1 is well able to capture the real angle. In Fig.8(d), the lumped disturbance z_3 is presented. Fig.8(e) shows the control inputs. The AAE and RMS values of the four methods are provided in Fig.9.

4) TRIANGULAR REFERENCE TRAJECTORY WITH LOAD

In the fourth experiment, a 2 kg load was added to the inner frame of the EOTS to check the robustness against uncertainties of the developed compound control strategy. The reference trajectory is the same as that used in the third experiment. In Fig.10(a), the trajectories with and without load track the predetermined reference trajectory with little error. Fig.10(b) shows the two tracking error curves. It can be seen that the tracking error with the load is slightly larger than that without the load. However, good control performance can still be obtained under an extra 2 kg load. Specifically, the with-load AAE increases by 0.2%. For RMS, the with-load result shows an increase of 0.2%. Fig.10(c) shows system state z_3, which estimates the lumped disturbance. Owing to the extra load, the lumped disturbance increases such that with-load z_3 is slightly larger than without-load z_3. Fig.10(d) presents the two control inputs. To ensure control accuracy with an extra load, the with-load control input requires a slightly larger control effort to handle the additional uncertainties. However, the two control inputs consume the same level of control torque. Fig.11 compares the AAE and RMS results with and without the load.

VI. CONCLUSION

This study proposed a nonlinear ESO based FO nonsingular terminal super-twisting SMC strategy designed for an EOTS with disturbances and unknown uncertainties. By applying the newly developed nonlinear ESO, the lumped disturbances of the system could be estimated without requiring explicit knowledge of the system model. The use of the NTSM guarantees the fast dynamical response of the control system. The use of FO calculus gives the controller a more flexible structure and a superior control and more robustness than its IO counterpart. In addition, the super-twisting sliding mode algorithm is integrated into the controller to increase the tracking accuracy and robustness. The finite-time convergence performance of both the developed nonlinear ESO and the system tracking error were analyzed using Lyapunov stability theory. Comparative experiments were conducted to evaluate the effectiveness of the developed control strategy, which was shown to be superior to the existing NTSM method in [38], the ESO+ISM method in [39], and the ESO+STA method in [40]. The results illustrate that our developed controller is capable of achieving faster response, higher tracking accuracy, and better robustness than the existing methods.

In future studies, we will consider integrating some adaptive laws into the developed controller to reduce the chattering, raise the tracking accuracy, and further improve the control performance.

REFERENCES

[1] S. P. Garaba, D. Voß, J. Wollschläger, and O. Zielinski, "Modern approaches to shipborne ocean color remote sensing," *Appl. Opt.*, vol. 54, no. 12, pp. 3602–3612, 2015.

[2] J. Zhang, Y. Liu, F. Zhang, S. Gao, and C. Han, "Digital sliding mode control via a novel reaching law and application in shipborne electro-optical systems," *IEEE Access*, vol. 7, pp. 139870–139884, Sep. 2019.

[3] A. Safa and R. Y. Abdolmaleki, "Robust output feedback tracking control for inertially stabilized platforms with matched and unmatched uncertainties," *IEEE Trans. Control Syst. Technol.*, vol. 27, no. 1, pp. 118–131, Jan. 2019.

[4] X. Wang, J. Liu, and Q. Zhou, "Real-time multi-target localization from unmanned aerial vehicles," *Sensors*, vol. 17, no. 12, p. 33, Dec. 2016.

[5] F. Yue and X. Li, "Robust adaptive integral backstepping control for opto-electronic tracking system based on modified LuGre friction model," *ISA Trans.*, vol. 80, pp. 312–321, Sep. 2018.

[6] Z. Xinli and X. Li, "A finite-time robust adaptive sliding mode control for electro-optical targeting system with friction compensation," *IEEE Access*, vol. 7, pp. 166318–166328, Nov. 2019.

[7] F. Yue and X. Li, "Adaptive sliding mode control based on friction compensation for opto-electronic tracking system using neural network approximations," *Nonlinear Dyn.*, vol. 96, no. 4, pp. 2601–2612, Jun. 2019.

[8] C. Bai and Z. Zhang, "A least mean square based active disturbance rejection control for an inertially stabilized platform," *Optik*, vol. 174, pp. 609–622, Dec. 2018.

[9] S. Cong, K. Deng, W. Shang, D. Kong, and H. Shen, "Isolation control for inertially stabilized platform based on nonlinear friction compensation," *Nonlinear Dyn.*, vol. 84, no. 3, pp. 1123–1133, May 2016.

[10] X. Zhou, H. Gao, B. Zhao, and L. Zhao, "A GA-based parameters tuning method for an ADRC controller of ISP for aerial remote sensing applications," *ISA Trans.*, vol. 81, pp. 318–328, Oct. 2018.

[11] M. Řezáč and Z. Hurák, "Structured MIMO design for dual-stage inertial stabilization: Case study for HIFOO and hinfstruct solvers," *Mechatronics*, vol. 23, no. 8, pp. 1084–1093, Dec. 2013.

[12] H. Pan, H. Li, W. Sun, and Z. Wang, "Adaptive fault-tolerant compensation control and its application to nonlinear suspension systems," *IEEE Trans. Syst., Man, Cybern. Syst.*, vol. 50, no. 5, pp. 1766–1776, May 2020.

[13] Z. Li, S. Zhou, Y. Xiao, and L. Wang, "Sensorless vector control of permanent magnet synchronous linear motor based on self-adaptive super-twisting sliding mode controller," *IEEE Access*, vol. 7, pp. 44998–45011, Apr. 2019.

[14] Q. Yao, "Adaptive finite-time sliding mode control design for finite-time fault-tolerant trajectory tracking of marine vehicles with input saturation," *J. Franklin Inst.*, vol. 357, no. 18, pp. 13593–13619, Dec. 2020.

[15] J. Baek, W. Kwon, and C. Kang, "A new widely and stably adaptive sliding-mode control with nonsingular terminal sliding variable for robot manipulators," *IEEE Access*, vol. 8, pp. 43443–43454, Mar. 2020.

[16] V.-C. Nguyen, A.-T. Vo, and H.-J. Kang, "A non-singular fast terminal sliding mode control based on third-order sliding mode observer for a class of second-order uncertain nonlinear systems and its application to robot manipulators," *IEEE Access*, vol. 8, pp. 78109–78120, Apr. 2020.

[17] V. Utkin, A. Poznyak, Y. Orlov, and A. Polyakov, "Conventional and high order sliding mode control," *J. Franklin Inst.*, vol. 357, no. 15, pp. 10244–10261, Oct. 2020.

[18] R. Cui, L. Chen, C. Yang, and M. Chen, "Extended state observer-based integral sliding mode control for an underwater robot with unknown disturbances and uncertain nonlinearities," *IEEE Trans. Ind. Electron.*, vol. 64, no. 8, pp. 6785–6795, Aug. 2017.

[19] A. Bartoszewicz and P. Latosinski, "Generalization of Gao's reaching law for higher relative degree sliding variables," *IEEE Trans. Autom. Control*, vol. 63, no. 9, pp. 3173–3179, Sep. 2018.

[20] X. Yao, J. H. Park, H. Dong, L. Guo, and X. Lin, "Robust adaptive nonsingular terminal sliding mode control for automatic train operation," *IEEE Trans. Syst., Man, Cybern. Syst.*, vol. 49, no. 12, pp. 2406–2415, Dec. 2019.

[21] B. Xu, R. Zhang, S. Li, W. He, and Z. Shi, "Composite neural learning-based nonsingular terminal sliding mode control of MEMS gyroscopes," *IEEE Trans. Neural Netw. Learn. Syst.*, vol. 31, no. 4, pp. 2406–2415, Apr. 2020.

[22] B. Ren, Y. Wang, and J. Chen, "A novel robust finite-time trajectory control with the high-order sliding mode for human-robot cooperation," *IEEE Access*, vol. 7, pp. 2169–3536, Sep. 2019.

[23] Z. Zhao, J. Yang, S. Li, Z. Zhang, and L. Guo, "Finite-time super-twisting sliding mode control for MARS entry trajectory tracking," *J. Franklin Inst.*, vol. 352, no. 11, pp. 5226–5248, Nov. 2015.

[24] H. N. Esfahani, R. Szlapczynski, and H. Ghaemi, "High performance super-twisting sliding mode control for a maritime autonomous surface ship (MASS) using ADP-based adaptive gains and time delay estimation," *Ocean Eng.*, vol. 191, Nov. 2019, Art. no. 106526.

[25] B. Yan, P. Dai, R. Liu, M. Xing, and S. Liu, "Adaptive super-twisting sliding mode control of variable sweep morphing aircraft," *Aerosp. Sci. Technol.*, vol. 92, pp. 198–210, Sep. 2019.

[26] J. Wang, C. Shao, and Y.-Q. Chen, "Fractional order sliding mode control via disturbance observer for a class of fractional order systems with mismatched disturbance," *Mechatronics*, vol. 53, pp. 8–19, Aug. 2018.

[27] R. Hu, H. Deng, and Y. Zhang, "Novel dynamic-sliding-mode-manifold-based continuous fractional-order nonsingular terminal sliding mode control for a class of second-order nonlinear systems," *IEEE Access*, vol. 8, pp. 19820–19829, Jan. 2020.

[28] Y. Wang, F. Yan, J. Chen, F. Ju, and B. Chen, "A new adaptive time-delay control scheme for cable-driven manipulators," *IEEE Trans. Ind. Informat.*, vol. 15, no. 6, pp. 3469–3481, Jun. 2019.

[29] Y. Wang, S. Jiang, B. Chen, and H. Wu, "A new continuous fractional-order nonsingular terminal sliding mode control for cable-driven manipulators," *Adv. Eng. Softw.*, vol. 119, pp. 21–29, May 2018.

[30] J. Han, "From PID to active disturbance rejection control," *IEEE Trans. Ind. Electron.*, vol. 56, no. 3, pp. 900–906, Mar. 2009.

[31] S. Ding, W.-H. Chen, K. Mei, and D. J. Murray-Smith, "Disturbance observer design for nonlinear systems represented by input–output models," *IEEE Trans. Ind. Electron.*, vol. 67, no. 2, pp. 1222–1232, Feb. 2020.

[32] H. Pan and W. Sun, "Nonlinear output feedback finite-time control for vehicle active suspension systems," *IEEE Trans. Ind. Informat.*, vol. 15, no. 4, pp. 2073–2082, Apr. 2019.

[33] H. Pan, X. Jing, and W. Sun, "Robust finite-time tracking control for nonlinear suspension systems via disturbance compensation," *Mech. Syst. Signal Process.*, vol. 88, pp. 49–61, May 2017.

[34] X. Zhou and X. Li, "Integral backstepping active disturbance rejection control strategy for the electro-optical targeting system," *J. Tianjin Univ.*, vol. 54, no. 4, pp. 379–387, 2021.

[35] J. Yao and W. Deng, "Active disturbance rejection adaptive control of hydraulic servo systems," *IEEE Trans. Ind. Electron.*, vol. 64, no. 10, pp. 8023–8032, Oct. 2017.

[36] B. Li, K. Qin, B. Xiao, and Y. Yang, "Finite-time extended state observer based fault tolerant output feedback control for attitude stabilization," *ISA Trans.*, vol. 91, pp. 11–20, Aug. 2019.

[37] H. Yang, X. Fan, P. Shi, and C. Hua, "Nonlinear control for tracking and obstacle avoidance of a wheeled mobile robot with nonholonomic constraint," *IEEE Trans. Control Syst. Technol.*, vol. 24, no. 2, pp. 741–746, Mar. 2016.

[38] S.-Y. Chen and F.-J. Lin, "Robust nonsingular terminal sliding-mode control for nonlinear magnetic bearing system," *IEEE Trans. Control Syst. Technol.*, vol. 19, no. 3, pp. 636–643, May 2011.

[39] L. Zhao, B. Zhang, H. Yang, and Y. Wang, "Observer-based integral sliding mode tracking control for a pneumatic cylinder with varying loads," *IEEE Trans. Syst., Man, Cybern. Syst.*, vol. 50, no. 7, pp. 2650–2658, Jul. 2020, doi: 10.1109/TSMC.2018.2825325.

[40] C. Ren, X. Li, X. Yang, and S. Ma, "Extended state observer-based sliding mode control of an omnidirectional mobile robot with friction compensation," *IEEE Trans. Ind. Electron.*, vol. 66, no. 12, pp. 9480–9489, Dec. 2019.

[41] T. Specker, M. Buchholz, and K. Dietmayer, "A new approach of dynamic friction modelling for simulation and observation," *IFAC Proc. Volumes*, vol. 47, no. 3, pp. 4523–4528, 2014.

[42] S. P. Bhat and D. S. Bernstein, "Finite-time stability of continuous autonomous systems," *SIAM J. Control Optim.*, vol. 38, no. 3, pp. 751–766, Jan. 2000.

[43] X. Wang and H. Lin, "Design and frequency analysis of continuous finite-time-convergent differentiator," *Aerosp. Sci. Technol.*, vol. 18, no. 1, pp. 69–78, Apr. 2012.

[44] J. A. Moreno, "A linear framework for the robust stability analysis of a generalized super-twisting algorithm," in *Proc. 6th Int. Conf. Electr. Eng., Comput. Sci. Autom. Control (CCE)*, Toluca, Mexico, Nov. 2009, pp. 1–6.

XINLI ZHOU received the B.S. degree in automation from the Wuhan University of Science and Technology, Hubei, China, in 2015, and the M.S. degree in instrumentation science and technology from Tianjin University, Tianjin, China, in 2018, where he is currently pursuing the Ph.D. degree in instrumentation science and technology.

His current research interests include robust control, active disturbance rejection control, electro-optical targeting systems, and fast-steering mirror systems.

XINGFEI LI received the M.S. degree in instrument science and technology from Southeast University, in 1994 and the Ph.D. degree from the College of Precision Instruments and Opto-Electronics Engineering, Tianjin University, Tianjin, China, in 2000. From 1996 to 1999, he worked as a Researcher with The Hong Kong Polytechnic University, Hong Kong, China. From 2003 to 2004, he did postdoctoral research in mechanical engineering with The University of Michigan, USA. He is currently a Professor with the College of Precision Instruments and Opto-Electronics Engineering, Tianjin University.

His research interests include nonlinear control, robust control, electro-optical targeting systems, signal processing, and manufacture and integration of inertial sensors.

● ● ●